

Astrocyte-Secreted Factors Modulate the Developmental Distribution of Inhibitory Synapses in Nucleus Laminaris of the Avian Auditory Brainstem

Matthew J. Korn,¹ Scott J. Koppel,¹ Lan H. Li,¹ Divya Mehta,¹ Sonia B. Mehta,¹ Armin H. Seidl,² and Karina S. Cramer^{1*}

¹Department of Neurobiology and Behavior, University of California at Irvine, Irvine, California 92697-4550

²Virginia Merrill Bloedel Hearing Research Center, University of Washington, Seattle, Washington 98195

ABSTRACT

Nucleus laminaris (NL) neurons in the avian auditory brainstem are coincidence detectors necessary for the computation of interaural time differences used in sound localization. In addition to their excitatory inputs from nucleus magnocellularis, NL neurons receive inhibitory inputs from the superior olivary nucleus (SON) that greatly improve coincidence detection in mature animals. The mechanisms that establish mature distributions of inhibitory inputs to NL are not known. We used the vesicular GABA transporter (VGAT) as a marker for inhibitory presynaptic terminals to study the development of inhibitory inputs to NL between embryonic day 9 (E9) and E17. VGAT immunofluorescent puncta were first seen sparsely in NL at E9. The density of VGAT puncta increased with development, first within the ventral NL neuropil region and subsequently throughout both the ventral and dorsal dendritic neuro-

pil, with significantly fewer terminals in the cell body region. A large increase in density occurred between E13–15 and E16–17, at a developmental stage when astrocytes that express glial fibrillary acidic protein (GFAP) become mature. We cultured E13 brainstem slices together with astrocyte-conditioned medium (ACM) obtained from E16 brainstems and found that ACM, but not control medium, increased the density of VGAT puncta. This increase was similar to that observed during normal development. Astrocyte-secreted factors interact with the terminal ends of SON axons to increase the number of GABAergic terminals. These data suggest that factors secreted from GFAP-positive astrocytes promote maturation of inhibitory pathways in the auditory brainstem. *J. Comp. Neurol.* 520:1262–1277, 2012.

© 2011 Wiley Periodicals, Inc.

INDEXING TERMS: astrocytes; inhibitory synapses; auditory brainstem; nucleus laminaris; synaptogenesis; superior olivary nucleus

Sensory systems require precise circuitry to represent and extract information from the environment. The avian auditory brainstem comprises a well-characterized circuit that uses temporal information to facilitate sound source localization. Auditory VIIIth nerve fibers contact neurons in ipsilateral nucleus magnocellularis (NM), which in turn project bilaterally to nucleus laminaris (NL) (Rubel and Parks, 1975; Jhaveri and Morest, 1982; Young and Rubel, 1983). Neurons in NL thus receive input from both NMs and act as coincidence detectors that respond maximally when information from both ears arrives simultaneously (Smith and Rubel, 1979; Overholt et al., 1992; Joseph and Hyson, 1993). Ipsilateral NM projections terminate on dorsal NL dendrites and NL cell bodies, while contralateral projections form delay lines that terminate on ventral

NL dendrites and cell bodies. This convergence of glutamatergic binaural inputs, together with properties including axon branch length and variations in myelination, is necessary for the computation of interaural time differences, essential for sound source localization (Carr and Konishi, 1990; Agmon-Snir et al., 1998; Cheng and Carr, 2007; Gorlich et al., 2010; Sanchez et al., 2010; Seidl et al., 2010).

Grant sponsor: National Institutes of Health (NIH); Grant numbers: NIH R01DC010796; Grant number: NIH P30DC008369; Grant sponsor: National Science Foundation (NSF); Grant number: NSF IOB-0642346.

*CORRESPONDENCE TO: Dr. Karina S. Cramer, Department of Neurobiology and Behavior, University of California, Irvine, CA 92697-4550. E-mail: cramerk@uci.edu

Received July 21, 2011; Revised September 2, 2011; Accepted October 4, 2011

DOI 10.1002/cne.22786

Published online 20 October 2011 in Wiley Online Library (wileyonlinelibrary.com)

© 2011 Wiley Periodicals, Inc.

The predominant source of inhibitory input to NL originates in the superior olivary nucleus (SON). SON provides inhibition directly to NL cell bodies and dendrites, NM, and nucleus angularis through a reciprocal pathway whereby NL neurons send projections to the ipsilateral SON (Lachica et al., 1994; Westerberg and Schwarz, 1995; Monsivais et al., 2000; Burger et al., 2005a; Tabor et al., 2010). These GABAergic afferents from SON improve phase locking in NM, enhance the ability of NL neurons to discriminate between sounds of short intervals, and enhance localization by making the system more responsive to variation in sound cues independent of sound intensity (Fujita and Konishi, 1991; Bruckner and Hyson, 1998; Yang et al., 1999; Nishino et al., 2008; Fukui et al., 2010; Tang et al., 2011).

Studies addressing the developmental emergence of inhibitory projections (Müller, 1987; Carr et al., 1989; Code et al., 1989; Code and Rubel, 1989; von Bartheld et al., 1989; Code and Churchill, 1991; Lachica et al., 1994; Burger et al., 2005a,b; Fukui et al., 2010) have demonstrated that inhibitory inputs arrive around embryonic day 12 (E12) and increase to mature levels by E17. A recent study examined the topography of projections from SON to NL in chick hatchlings, noting that presynaptic terminals were located along the dorsal and ventral dendrites, as well as cell bodies within NL (Tabor et al., 2010). Additionally, Tang et al. (2011) described the distribution of a subpopulation of GABA_A receptors containing the δ subunit throughout NL in posthatch chicks as being present mainly on NL somata and diffuse throughout the neuropil. Characterization of the developmental distribution of SON inputs to distinct regions of NL neurons will enhance our understanding of mechanisms that guide the formation of this inhibitory pathway.

In order to further elucidate the interactions necessary for the maturation of inhibitory terminals on NL cells, we examined the normal distribution and density of inhibitory presynaptic sites during embryonic development. We report here that substantial changes in these distributions occur at a time that coincides with astrocyte maturation in NL (Korn and Cramer, 2008). This late stage increase in inhibitory inputs suggests the possibility that brainstem glia play a role inhibitory synaptogenesis.

Several studies have demonstrated that glial cells can promote the formation of inhibitory synapses on dissociated hippocampal neurons (Liu et al., 1996, 1997; Elmariah et al., 2004, 2005a,b; Hughes et al., 2010). However, the general importance of glial cells for the formation of inhibitory inputs in intact neural circuits remains relatively unexplored. Here we investigated the role of glial cells in the maturation of the inhibitory pathway from SON to NL. Glial cells populate the area around NL in the avian auditory brainstem (Lippe et al., 1980; Deitch and Rubel,

1989; Lurie and Rubel, 1994; Lurie et al., 2000; Feng and Morest, 2006) and glial fibrillary acidic protein (GFAP)-positive astrocytes can first be identified at E15, just ventral to NL (Korn and Cramer, 2008). By E17 these astrocytes surround the NL cell layer and their processes can be found throughout the neuropil and cell bodies. We developed an organotypic slice preparation to test whether secreted factors from GFAP-positive astrocytes play a role in inhibitory synaptogenesis in the avian auditory brainstem. Our results suggest that molecules secreted from mature astrocytes promote inhibitory synaptogenesis during late embryonic development in the avian auditory brainstem.

MATERIALS AND METHODS

Animals

Fertilized white leghorn eggs (AA Laboratories, Westminster, CA) were set in a rotating incubator at 39°C and used prior to hatching at ages E9–17. Unless otherwise noted, brainstems were rinsed in 0.1 M phosphate buffer (PB), pH 7.4, and fixed for 25 minutes in 4% paraformaldehyde (PFA), cryoprotected overnight in 30% sucrose at 4°C, and cryosectioned at 25 μ m in the coronal plane using a Leica CM1850 cryostat (Leica Microsystems, St. Louis, MO). In some instances we sectioned brainstems 30° from to the sagittal plane to collect slices that contained the majority of the tonotopic (rostromedial to caudolateral) extent of NL (Rubel and Parks, 1975; Person et al., 2004).

Dissociated astrocyte culture and collection of conditioned medium

Astrocyte isolation was adapted from previous studies (Taylor et al., 2007). Briefly, E16 brainstems were trypsinized (0.05% trypsin-EDTA) and the tissue was dissociated in DMEM/F12 containing penicillin/streptomycin (astrocyte base media; ABM) with 10% fetal bovine serum (astrocyte growth media; AGM) and 100 μ l of bovine serum albumin (BSA). The resulting supernatant was layered above AGM containing 4% BSA and briefly centrifuged. The pellet containing the dissociated cells was resuspended in AGM, poured through a 40- μ m cell strainer, and transferred to a T-75 flask pretreated with poly-d-lysine (50 μ g/ml; Sigma-Aldrich, St. Louis, MO), with media replaced every 48 hours until cultures were confluent.

To produce fibrous astrocytes, confluent flasks were treated with 1 μ M cytosine arabinoside in ABM for 24 hours. The cells were then replated in ABM containing G5 Neuroplex supplement (1:100; 500 g/ml insulin, 5 mg/ml human transferrin, 0.52 g/ml selenite, 1 g/ml biotin, 0.36 g/ml hydrocortisone, 0.52 g/ml FGF₂, and 1 g/ml

EGF, ADM; Gemini Bio-Products, West Sacramento, CA) at 3×10^6 cells per T-75 flask. Once confluent, the cultures were exchanged to ABM (without G5) to collect astrocyte-secreted factors for 3–4 days. The astrocyte conditioned medium (ACM) was concentrated using an Amicon Ultra 10K centrifugal filter (Millipore, County Cork, Ireland) and assayed for protein concentration.

Organotypic slice preparation

Our protocol for preparing organotypic brainstem slices was modified from previous studies (Seidl and Rubel, 2009; Sanchez et al., 2011). Physiological properties of chick auditory brainstem neurons have been previously shown to be preserved *in vitro* (Kuenzel et al., 2007). Embryos were removed at E13 and dissected so as to keep the brainstem together with cochlea, cochlear ganglion, and VIIIth nerve intact. We included these peripheral structures and innervation to prevent effects of deaf-ferentation on the number and density of inhibitory terminals in NL (Deitch and Rubel, 1989; Sorensen and Rubel, 2006). The tissue was immediately placed into cold culture medium containing 50% advanced minimum essential media (MEM; Invitrogen, Carlsbad, CA), 25% Earle's balanced salt solution (EBSS; Sigma-Aldrich), 25% normal horse serum (NHS, heat-inactivated and filter sterilized; Invitrogen), supplemented with 200 mM L-glutamine (Sigma-Aldrich), D-glucose (5.5 mg/ml; Sigma-Aldrich), penicillin and streptomycin (10,000 unit/ml, 10,000 μ g/ml; Invitrogen). After a brief rinse, tissue was placed in 4% low-melting point agarose in artificial cerebrospinal fluid (ACSF; 130 mM NaCl, 3 mM KCl, 1.2 mM KH_2PO_4 , 20 mM NaHCO_3 , 3 mM HEPES, 10 mM glucose, 2 mM CaCl_2 , 1.3 mM MgSO_4) perfused with 95% O_2 and 5% CO_2 , and sectioned at 400 μ m on ice using a VT1000P Vibratome (Leica Microsystems).

Each brainstem yielded two to three sections roughly corresponding to the rostral, middle, or caudal region of the auditory brainstem. Slices were then transferred to a 0.4 μ m membrane Millicell-CM culture plate insert (Millipore) pretreated with 200 μ l of a 0.01% polyornithine solution (Sigma-Aldrich). Each membrane contained two slices and the insert was placed in a 3.46-cm diameter well with 1 ml of control culture media (as described above). For proper adhesion to membrane inserts, slices required equilibration for 24 hours prior to the first media exchange. The following day, wells were selected at random to receive a fresh exchange of either control medium or control medium supplemented with concentrated ACM (mixed 1:1). We report a single 24-hour period of treatment with ACM supplemented medium or control medium as +1 day *in vitro* (DIV).

Following the conclusion of treatment, slices were fixed on the culture plate insert for 25 minutes. They

were then rinsed in PB, cryoprotected in a 1.55-cm diameter well containing 30% sucrose, and cryosectioned at 30 μ m. Resectioning was performed to optimize penetration of antibodies in immunofluorescence procedures.

Heparin-acrylic beads

Heparin-acrylic beads were prepared according to our previously published protocol (Korn and Cramer, 2007). For these experiments, beads 50–100 μ m in diameter were rinsed with dPBS and MEM, resuspended, and soaked overnight at 37°C in 50 μ l of 150–200 μ g/ml ACM or control medium. A single bead was placed no further than 200 μ m ventral from NL. Immunohistochemistry for neurofilament was used to ascertain that the SON afferent pathway remained intact and Nissl stain was used to verify that beads did not distort the NL cell layer.

In vitro labeling

To quantify the number of VGAT puncta aligned with NL dendrites, we labeled individual NL neurons with rhodamine dextran amine (RDA; MW = 3000; Molecular Probes, Eugene, OR; 8–10% in sterile saline). Vibratome sections were made in cold oxygenated ACSF at 150 μ m and fixed immediately following dye injection. Neurons were filled iontophoretically as previously described (Sorensen and Rubel, 2006) using a charged platform and a dye-filled electrode controlled by a BTX Electro Square Porator ECM 830 (Harvard Apparatus, Dover, MA).

Immunolabeling and antibodies characterization

Sections were rinsed in PB and blocked for 35 minutes with 5% normal horse serum containing 0.01% Triton in PB. For VGAT, sections were incubated overnight at 4°C; for neurofilament slides were incubated at room temperature. See Table 1 for a list of antibody specifications and dilutions.

VGAT

Rabbit anti-vesicular GABA amino acid transport polyclonal antibody (VGAT, 2100-VGAT; lot aj0806p; PhosphoSolutions, Aurora, CO) was raised against a peptide fragment corresponding to a 17 amino acid sequence (VHSLEGLIEAYRTNAED) from the N-terminal region of rat VGAT. Antibody specificity was confirmed by western blot analysis of whole brain isolate, PC12 cells expressing the protein and rat hippocampal lysate, all confirming immunolabeling of a 53–57 kD protein corresponding to VGAT (manufacturer's technical information; Chaudhry et al., 1998). We used VGAT immunofluorescence for the identification of GABAergic presynaptic terminals, as it is responsible for packaging inhibitory neurotransmitters into

TABLE 1.
Specifications of Antibodies Used

Antigen	Immunogen	Manufacturer; species in which anti-body was raised; mono- vs. polyclonal; catalog no.; lot no.	Dilution Used
Vesicular GABA amino acid transport (VGAT)	Rat brain, peptide fragment containing the amino acids VHSLEGLIEAYRTNAED from the N-terminal region.	PhosphoSolutions; rabbit; polyclonal; 2100-VGAT; aj0806p	1:600
Neurofilament H	Rat brain, NF-H fusion protein containing 37 lysine-serine-proline (KSP) tandem repeats near NF-H tail containing the consensus AKSPAEE.	Millipore; rabbit; polyclonal; AB-1991; NG17211775	1:500

synaptic vesicles. The labeling patterns described here are similar to previous studies that localized VGAT in the mature NL of the chick (Nishino et al., 2008).

Neurofilament

Rabbit polyclonal anti-neurofilament H (NF, AB-1991; lot NG17211775; Millipore, Bedford, MA) was generated using an *E. coli* recombinant fusion protein developed against the first 704 basepairs of the rat NF-H cDNA isolated by Lieberburg et al. (1989). The resulting fusion protein contained 37 lysine-serine-proline (KSP) repeats of the rat NF-H protein, which contains the consensus amino acid sequence AKSPAEE, located near the N-terminus of the rat NF-H tail (Harris et al., 1991). The H-chain is one of the three intermediate filaments comprising the neurofilaments that are localized to neurons and their axons. The manufacturer cites especially strong reactivity to the major NF subunit NF-H, with additional reactivity to NF-M, as it also contains several KSP repeats. The observed filament labeling described here is very similar to previous reports of immunoreactivity of neurofilament in the developing chick auditory brainstem (Hendricks et al., 2006).

Imaging and analysis

To evaluate the distribution of inhibitory synapses, sections were viewed on a Zeiss AxioSkop epifluorescence microscope (Carl Zeiss, Thornwood, NY) and the auditory brainstem was imaged at 20 \times magnification with a digital camera and processed using Zeiss OpenLab software.

Regions of NL were identified using the differential interference contrast, first by locating the cell layer and then the cell body-free neuropil. Photos were made such that the most dense VGAT labeling was in focus. Density measurements were made by sampling a single focal plane of each section. Once we determined the border of each region, a grid composed of 20 μm^2 squares was placed over the image using ImageJ 1.44 (NIH, Bethesda,

MD; Fig. 1A). Squares containing the designated portion of the neuron were numbered and three squares within each region were selected for counting using a random number generator (Fig. 1B).

Using the grid as a guide, contours were drawn so that the counting frame was restricted to an area within the cell body layer, the dorsal neuropil, or the ventral neuropil (Fig. 1B). We calculated the density as puncta within the frame and report the density as puncta per 400 μm^2 . To be included each image was required to have 700 μm^2 or more of measured surface area in each region.

Each selected area was enhanced 2 \times using the digital zoom feature in ImageJ (Fig. 1B). Further inclusion criteria for puncta considered size, shape, and location. Puncta smaller than 1.0 μm and those on the gridline were not counted. In the case of contiguous labeling or clusters, only clearly defined spherical or ovoid puncta whose intensity level fit a normal distribution across the length of the labeled area were counted (Fig. 1B'). Synaptic puncta labeling could be easily distinguished from background scatter using our criteria. Three individuals quantified puncta independently and blind to age or treatment group. Their numbers were verified for consistency and found to vary less than one punctum per sampling region.

To report the density of VGAT puncta during normal development, two left and right sides were selected at random, averaged together, and a single density was determined for each NL region for each brain. This procedure also provided samples of the density throughout the extent of the tonotopic axis. For *in vitro* experiments, each side was averaged separately to account for any variations in the plane of Vibratome sectioning or loss of one side during cryostat resectioning. Only measurements from sections that had continuous labeling throughout NL were used to determine the average density, reducing the possibility of sampling regions with SON axons cut during preparation (Fig. 1C).

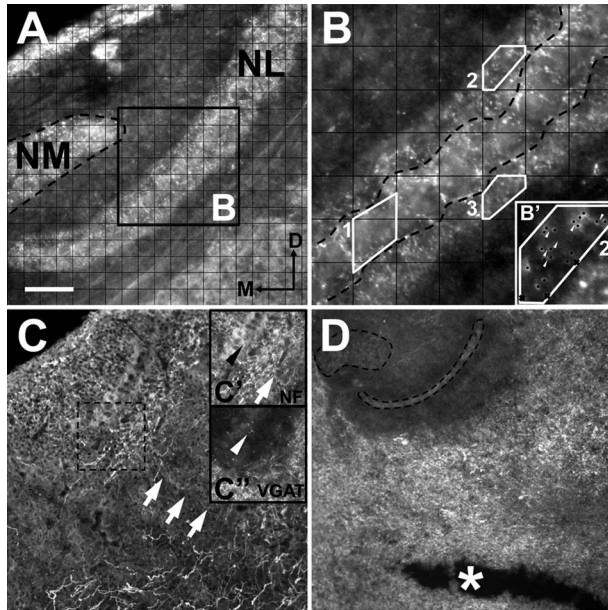


Figure 1. Image analysis of VGAT labeling in vivo (A,B) and in vitro (C,D). **A:** Dorsal portion of the right side of the avian auditory brainstem containing nucleus magnocellularis (NM) and nucleus laminaris (NL) with VGAT labeling. A grid of $20\ \mu\text{m}^2$ squares was used to establish sampling counting frames across the entire mediolateral extension of NL. **B:** A $2\times$ digital enhancement of the black frame in A. Once counted off, three grid squares were selected using a random number generator from each region (examples 1–3, separated by dashed black line) and contours (white outlines) were drawn so that the counting frame included only area within the cell body layer (contour 1), the dorsal neuropil (contour 2), or the ventral neuropil (contour 3). Puncta (black dots in B') were identified using conservative criteria that excluded puncta out of focus and those along the contours (black cross in B'). Punctum were counted so long as a discontinuity was identifiable between labeled points (white arrowheads). **C:** Neurofilament (NF)-positive fibers (white arrows in C and C') from the ventral portion of the brainstem contain VGAT puncta (white arrowhead in C') on their terminal ends (black arrowhead in C'). Cultured slices were excluded if VGAT labeling was not continuous throughout NL (as with C'). **D:** A horizontal cut (asterisk) ventral of NL interrupts GABAergic axons from the SON and results in an absence of VGAT labeling within NM and NL. Dorsal is up in all figures and medial is to the left when one side is shown. Scale bar = $60\ \mu\text{m}$ for A,C,C'; $20\ \mu\text{m}$ for B; $40\ \mu\text{m}$ for B'; $160\ \mu\text{m}$ for C,D.

Two-photon microscopy

To determine the linear density of VGAT puncta apposed to labeled NL dendrites, we used a custom-made video-rate two-photon laser scanning microscope, as described previously (Nguyen et al., 2001; Stutzmann et al., 2003; Stutzmann and Parker, 2005). Briefly, excitation was provided by trains of 100 fs pulses at 750–800 nm from a Chameleon Ti:sapphire laser (Coherent, Santa Clara, CA). The laser beam was scanned at 30 frames per second and focused through a $20\times$ water-immersion

objective [numerical aperture (NA) 0.95], or $40\times$ water-immersion objective (NA 0.8) on an upright microscope (Olympus BX51WIF, Olympus America, Center Valley, PA). Emitted fluorescence light was detected by photomultipliers (Hamamatsu, Middlesex, NJ) to derive a video signal that was captured and analyzed using SlideBook 5.0 (Intelligent Imaging Innovations, Santa Monica, CA). Z-stacks were acquired at $1\ \mu\text{m}$ per plane, 3D-rendered, and analyzed. Initially neurons were viewed using only the red channel (filled NL dendrites) to prevent a selection bias. Three continuous dendritic segments of $5\ \mu\text{m}$ or greater were selected at random and measured, then using only the green channel (VGAT labeling) we measured the length of the segment in direct apposition to VGAT puncta. To be considered in direct apposition, puncta had to match the contour of the filled dendrites. We reported apposition as a percent of dendritic length.

Representative images of labeling were exported as TIFF files and edited using Jasc Photo Shop Pro 8 (Corel, Ottawa, Ontario, Canada). In some instances brightness and contrast were adjusted to reduce background labeling. Images were converted to grayscale, resized to 300 dpi, and cropped to fit the dimensions of each figure.

Statistics

All statistical evaluations were made using JMP 9 software (SAS, Cary, NC). Datasets were checked for normal distributions. Analysis of variance (ANOVA) was performed to assess differences across multiple comparisons. Unless otherwise noted, individual comparisons were made using Tukey's HSD test to correct for sample number. In some circumstances we performed a nonparametric comparison using Wilcoxon's *t*-test. When appropriate, we performed a paired *t*-test. Values are reported as mean \pm SEM. In figures, a single asterisk represents a statistical significance of $P < 0.05$, two asterisks $P < 0.005$, and three asterisks $P < 0.0005$.

RESULTS

Normal developmental distribution of VGAT VGAT density at E9

Consistent with previous observations regarding the presence of inhibitory terminals in NL (Code et al., 1989), the earliest age that we detected VGAT immunoreactivity was E9 ($n = 5$; Fig. 2A). At this age the NL cell layer is not yet fully separated from NM, nor has the cell layer taken on its characteristic laminar appearance (Rubel et al., 1976; Book and Morest, 1990; Hendricks et al., 2006). However, we were still able to count puncta in direct contact with NL cell bodies (3.77 ± 0.91 per $400\ \mu\text{m}^2$) and those adjacent to the forming neuropil (6.87 ± 1.17).

VGAT density from E10–12

Our systematic analysis of the puncta density in distinct NL compartments began at E10, when the NL neuropil becomes identifiable and NL cell bodies form a single-cell lamina. Inhibitory terminals could be found throughout NL at E10–12 ($n = 12$; Fig. 2B,E). Most notable at this age was a distinctly polarized distribution of VGAT puncta within the ventral NL neuropil (8.53 ± 0.40 per $400 \mu\text{m}^2$; Fig. 2B). This density was significantly greater than that seen on the cell bodies (3.44 ± 0.21 , $P < 0.0002$; Fig. 2E) and the dorsal dendritic region (4.76 ± 0.51 , $P < 0.0002$, paired t -test; Fig. 2E). There was no significant

difference in the density along the tonotopic axis within the cell body region ($P = 0.89$), the dorsal neuropil ($P = 0.40$), or the ventral neuropil ($P = 0.90$).

VGAT density from E13–15

We observed a significant increase in the density of inhibitory presynaptic puncta throughout NL in animals between the ages of E13–15 ($n = 46$; Fig. 2C,E,F). The density of puncta in the ventral neuropil was 16.43 ± 0.42 per $400 \mu\text{m}^2$, which represents a nearly 2-fold increase compared to the density of terminals within the ventral dendritic region at E10–12 ($P < 0.0002$; Fig. 2F). Although we observed about a 2.5-fold increase in the cell body region (to 8.76 ± 0.44 , $P < 0.002$; Fig. 2F) and 3-fold increase within the dorsal dendritic region (to

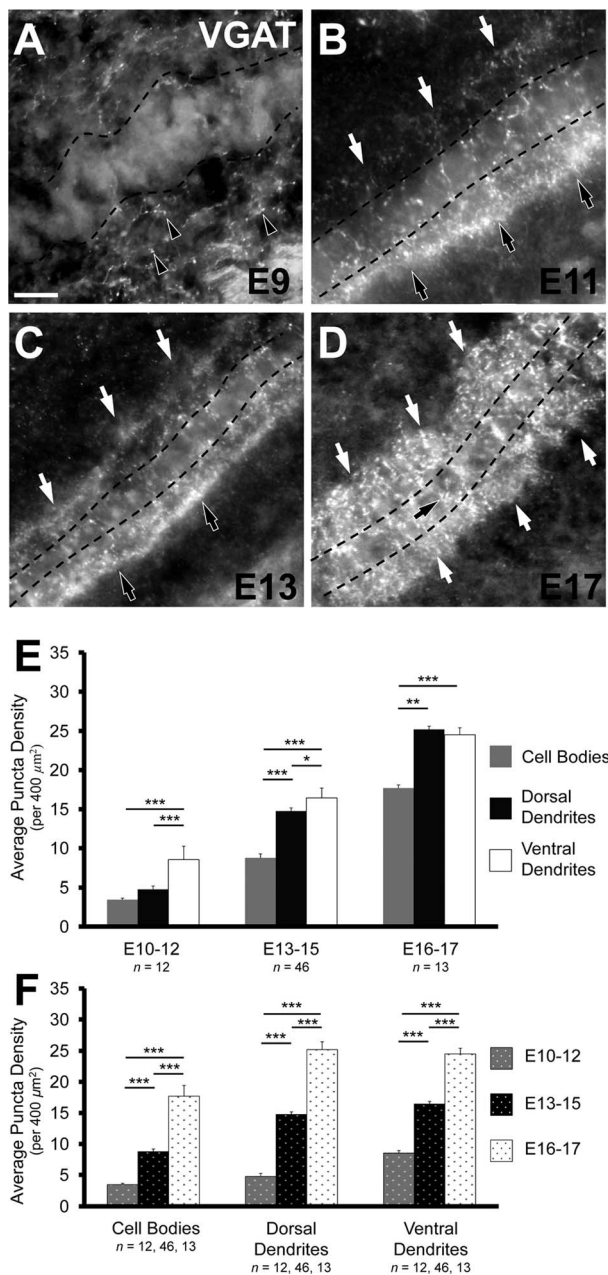


Figure 2

Figure 2. Inhibitory terminals in NL during development. **A:** Inhibitory inputs are first seen at E9 and are predominately located ventral (black arrowheads) to the forming NL cell layer. **B:** The NL neuropil and cell body layer are readily identifiable (cell layer outlined by dashed line) in E11 brainstems. Inhibitory terminals exhibit a distinctly polarized distribution in the ventral neuropil (black arrows), but are also located throughout NL cell bodies and the dorsal neuropil (white arrows). **C:** VGAT density increases in NL at E13–15 (represented here by E13), but the asymmetry between ventral (black arrows) and dorsal (white arrows) dendritic region remains apparent. **D:** A further increase in inhibitory terminals is evident at E16–17 (represented here by E17). VGAT puncta are distributed similarly in the ventral and dorsal neuropil regions (white arrows), although there remain notably fewer puncta on the cell bodies (black arrow). **E:** Comparison of the distribution of VGAT puncta in each of the three age groups. In the E10–12 age group there is a significantly greater density in the ventral dendritic region (8.53 ± 0.40 per $400 \mu\text{m}^2$) compared to that of the dorsal dendritic region (4.76 ± 0.51 , $P < 0.0002$, paired t -test) and cell body region (3.44 ± 0.21 , $P < 0.0002$). At E13–15 the ventral neuropil (16.43 ± 0.42) has a significantly greater density than both the dorsal neuropil (14.76 ± 0.40 , $P < 0.0002$, Wilcoxon T) and cell body region (8.76 ± 0.44 , $P < 0.002$). In this age group the dorsal dendritic region has a significantly greater density than the cell body region ($P < 0.0002$). At E16–17 the density of VGAT in both the ventral and dorsal neuropil are significantly greater than the density in the cell body region (17.7 ± 1.72 , $P < 0.02$ and $P < 0.002$, respectively). The density in the ventral neuropil (24.51 ± 0.90) and dorsal neuropil (25.19 ± 1.27) do not differ significantly ($P = 0.93$). **F:** Change in density of VGAT puncta in each region during development. In the cell body region, both the increases from E10–12 (3.44 ± 0.21 per $400 \mu\text{m}^2$) to E13–15 (8.76 ± 0.44) and E13–15 to E16–17 (8.76 ± 0.44) are significant ($P < 0.0002$ and $P < 0.0002$, respectively). The increases in density in the ventral neuropil from E10–12 (8.53 ± 0.40) to E13–15 (16.43 ± 0.42) and E13–15 to E16–17 (24.51 ± 0.90) are significantly different (for all comparisons $P < 0.0002$, Wilcoxon T). Similar increases are seen in the dorsal dendritic region from E10–12 (4.76 ± 0.51) to E13–15 (14.76 ± 0.40) and E13–15 to E16–17 (25.19 ± 1.27 , $P < 0.0002$). For E,F, * $P < 0.05$, ** $P < 0.005$, *** $P < 0.0005$. Scale bar = $20 \mu\text{m}$.

14.76 ± 0.40, $P < 0.0002$, Wilcoxon T; Fig. 2F), the ventral dendritic region maintained a significantly greater density compared to cell bodies ($P < 0.0002$; Fig. 2E) and dorsal dendrites ($P < 0.0002$, paired t -test; Fig. 2E) at this age. There was no significant difference in the density along the tonotopic axis within the cell body region ($P = 0.91$), the dorsal neuropil ($P = 0.44$), or ventral neuropil ($P = 0.86$).

VGAT density from E15–17

VGAT density further increased from E13–15 to E16–17 ($n = 13$; Fig. 2D–F). This developmentally most advanced group tested represents the greatest density observed in our study and the general distribution is similar to that reported in posthatch animals (Nishino et al., 2008; Tabor et al., 2010; Tang et al., 2011). We observed a 1.5-fold increase in the ventral dendritic region (24.51 ± 0.90 per $400 \mu\text{m}^2$, $P < 0.0002$; Fig. 2F), almost a 2-fold increase in the dorsal dendritic region (25.19 ± 1.27 , $P < 0.0002$; Fig. 2F), and a 2-fold increase in the cell body region (17.7 ± 1.72 , $P < 0.0002$; Fig. 2F). This differential increase across NL resulted in similar densities of VGAT puncta in the dorsal and ventral neuropil ($P = 0.93$), while VGAT puncta were significantly less dense in the cell body layer ($P < 0.002$ and $P < 0.02$, for dorsal and ventral neuropil, respectively, compared to cell bodies; Fig. 2E). There was no significant difference in the density along the tonotopic axis within the cell body region ($P = 0.41$), the dorsal neuropil ($P = 0.64$), or ventral neuropil ($P = 0.47$). Uniformity along the tonotopic axis was also seen in brainstem slices that contained the entire extent of NL ($n = 5$; Fig. 3A). The density within the cell body region ranged between 10–12 puncta per $400 \mu\text{m}^2$ ($P = 0.53$; Fig. 3B), 14–18 puncta within the dorsal neuropil ($P = 0.08$; Fig. 3B), and 15–19 in the ventral neuropil ($P = 0.33$; Fig. 3B).

VGAT apposition along NL dendrites

We next determined whether the increase in VGAT puncta correlated with the number of terminals apposed to postsynaptic dendrites. Due to the paucity of puncta in the dorsal neuropil at E10–12 ($n = 6$ neurons), we only measured apposition on the ventral dendrites at this age. We found that only about a quarter of the dorsal dendritic length was apposed by VGAT puncta ($27.2 \pm 3.9\%$; Fig. 4A). The increase in apposition in the E13–15 ($n = 9$) age group ($38.3 \pm 1.6\%$; Fig. 4B) was not significant ($P = 0.053$). From E13–15 to E16 and E17 ($n = 7$) there was a greater than 1.5-fold increase in the percent apposition of VGAT to dendritic length ($64.3 \pm 4.1\%$; Fig. 4C). This increase in NL apposition from the previous age group was significant ($P < 0.0002$; Fig. 4D), suggesting that the developmental period from E13–15 to E16–17 represents a major phase of inhibitory synaptogenesis.

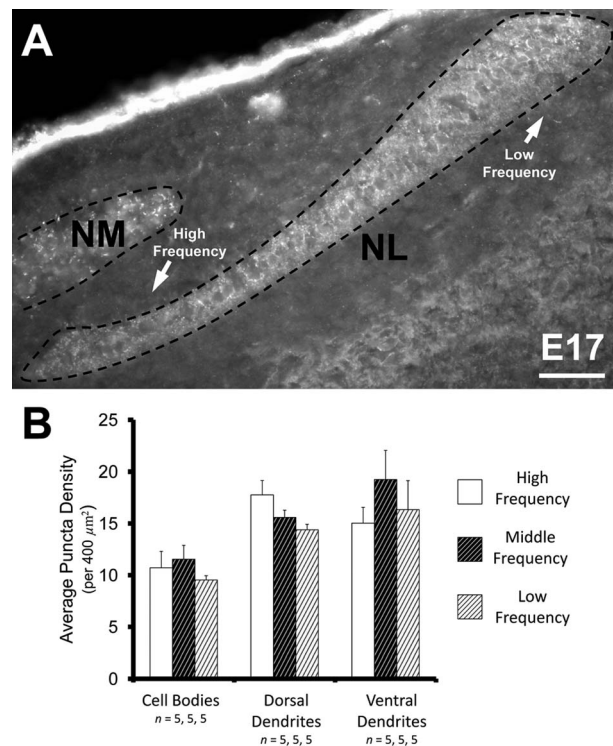


Figure 3. Inhibitory terminals in NL along the tonotopic axis. **A:** The distribution of inhibitory synapses is relatively consistent throughout NL, from the rostromedial to caudolateral extent. **B:** As with earlier ages, the density of VGAT does not vary along the tonotopic axis at E17. The density within the cell body region in the high-frequency (10.72 ± 1.60 per $400 \mu\text{m}^2$), the middle-frequency (11.56 ± 1.33), and the low-frequency (9.55 ± 0.41) neurons were not different from one another ($P = 0.53$). The density within the dorsal dendrite region in the high-frequency (17.77 ± 1.40), the middle-frequency (15.60 ± 0.70), and the low-frequency (14.40 ± 0.53) neurons were also not different from one another ($P = 0.08$). Lastly, the density within the ventral dendrite region in the high-frequency (15.03 ± 1.54), the middle-frequency (19.26 ± 2.79), and the low-frequency (16.35 ± 2.80) neurons were not different from one another ($P = 0.33$). Scale bar = $50 \mu\text{m}$.

The increase in the percent of NL dendritic length contacted by VGAT puncta is not due to changes in puncta size, as the distribution of the size of the VGAT-positive puncta was the same at each age (range: 1.3–2.3 μm in diameter, ANOVA, $P = 0.21$; Fig. 4E). The sharp increase in inhibitory synaptic sites in NL after E15 occurs at a time when GFAP-positive astrocytes mature in NL (Korn and Cramer, 2008). The second part of our study examines the affect of ACM on the maturation of inhibitory synapses during this period of development.

Distribution of VGAT *in vitro*

Astrocyte-secreted factors on VGAT density *in vitro*

The observation that inhibitory presynaptic terminals increase in density after maturation of GFAP-positive

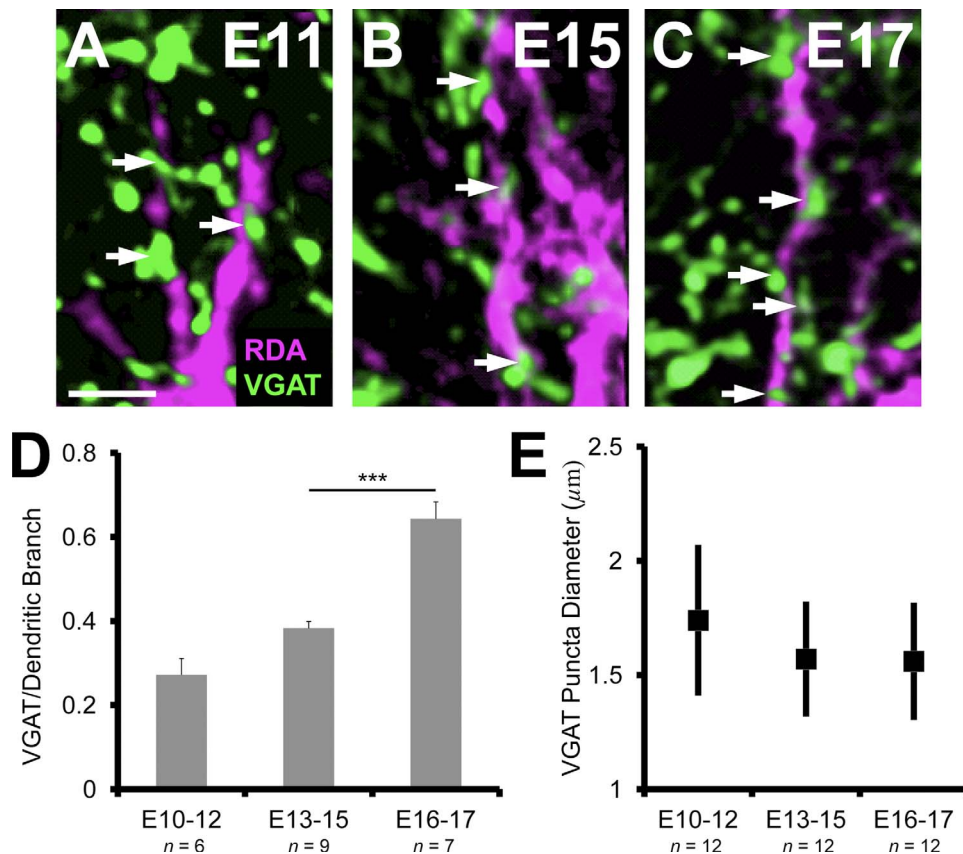


Figure 4. VGAT apposition along NL dendrites increases at late embryonic ages. A–C: The progressive increase in the number of VGAT puncta (white arrows) per unit length (μm) of NL dendrite between E11 and E17. D: The increase from E10–12 ($27.2 \pm 3.9\%$) to E13–15 ($38.3 \pm 1.6\%$) is not significant ($P = 0.053$). The number of VGAT apposed to dendrites at E16–17 ($64.3 \pm 4.1\%$) is significantly greater ($P < 0.0002$) than previous ages, suggesting a key phase in inhibitory synapse development. E: The range in puncta size did not change over age ($1.3\text{--}2.3 \mu\text{m}$ in diameter, ANOVA, $P = 0.21$). Scale bars = $10 \mu\text{m}$.

fibrous astrocytes at E15 is consistent with a role for these glial cells in promoting maturation of inhibitory synapses. Our organotypic culture preparation contains intact inhibitory projections from the SON that have terminals located in the vicinity of NL several days before GFAP-astrocytes can be detected. To test whether astrocyte-derived factors promote formation of inhibitory synapses, we treated cultured slices containing SON and NL with ACM derived from E16 brainstem astrocytes and compared the density of VGAT puncta in NL with VGAT density in tissue treated with control medium.

In organotypic slices incubated in control medium for +1 DIV the relative proportions of VGAT puncta in the ventral neuropil, dorsal neuropil, and cell body layer were similar to the proportions seen at E13–15. Ventral neuropil had $39.4 \pm 1.6\%$ of total puncta in vitro and $41.4 \pm 0.6\%$ of puncta at E13–15 ($P = 0.59$). Likewise, dorsal dendrites had $35.3 \pm 1.0\%$ of total puncta in vitro and $37.1 \pm 0.6\%$ of puncta at E13–15 ($P = 0.55$), and the cell body layer had $25.4 \pm 1.6\%$ of total puncta in vitro and $21.5 \pm 0.6\%$ of puncta at E13–15 ($P = 0.06$; compare

Fig. 2E at E13–15 and 5E). The ventral neuropil had a significantly greater density (6.21 ± 0.43 per $400 \mu\text{m}^2$; Fig. 5A,E) than both the dorsal neuropil (5.61 ± 0.35 , $P < 0.05$, paired *t*-test; Fig. 5A,B,E) and cell body region (4.25 ± 0.45 , $P < 0.02$; Fig. 5A,B,5E).

Compared to controls, slices treated for +1 DIV with ACM ($n = 18$) had a significantly greater density in both the ventral (10.83 ± 0.88 , $P < 0.0002$; Fig. 5B,D,E) and dorsal dendritic neuropil (10.48 ± 0.97 , $P < 0.0002$; Fig. 5B,D,E). The increase in VGAT density in the cell body region was not significant (6.19 ± 0.84 , $P = 0.10$, Wilcoxon T; Fig. 5E). Both the dorsal and ventral dendritic neuropil exhibited a significantly greater density compared to the cell body layer ($P < 0.02$ and $P < 0.002$, respectively). Also, the percent distributions in both the ventral ($40.3 \pm 0.9\%$) and dorsal ($38.3 \pm 1.2\%$) dendritic regions were not different from one another ($P = 0.12$, paired *t*-test). These distributions were similar to those of E16–17 animal (dorsal neuropil: $37.4 \pm 0.9\%$, $P = 0.95$; ventral neuropil: $36.9 \pm 1.4\%$, $P = 0.18$; compare Fig. 2E at E16–17 and 5E).

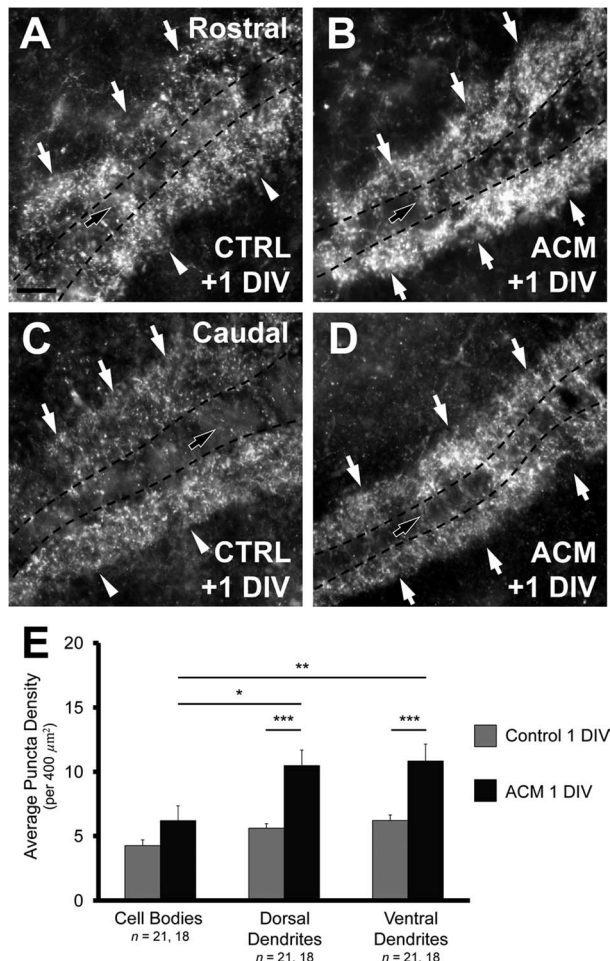


Figure 5. Astrocyte-secreted factors increase the density of VGAT in vitro. **A:** Rostral slices (see Materials and Methods) after +1 DIV with control medium exhibit a distribution of VGAT density similar to that observed in vivo at E13–15 with a greater density of inhibitory synapses in the ventral neuropil (white arrowheads) than in the dorsal neuropil (white arrows), and cell body region (black arrow). **B:** Rostral slices treated with ACM for +1 DIV exhibit an increase in VGAT density in the dorsal and ventral neuropil (white arrows). ACM does not increase the number of inhibitory terminals within the cell body region (black arrow). **C:** Caudal slices (see Materials and Methods) incubated for +1 DIV with control medium exhibit the same polarized distribution in the ventral neuropil (white arrowheads). **D:** The density of VGAT within the dorsal and ventral dendritic regions of caudal slices also increases after +1 DIV with ACM, but not on the cell bodies (black arrow). In both B,D, the increase is such that both dorsal and ventral dendritic regions exhibit similar inhibitory terminal density (white arrows). **E:** Change in density after +1 DIV with ACM compared to controls in each NL region. Slices treated with ACM had a significantly greater density in both the ventral (from 6.21 ± 0.43 puncta per $400 \mu\text{m}^2$ to 10.83 ± 0.88 , $P < 0.0002$) and dorsal dendritic region (from 5.61 ± 0.35 to 10.48 ± 0.97 , $P < 0.0002$) compared to control slices. The difference between the density in the cell body region of treated and control slice was not different (from 4.25 ± 0.45 to 6.19 ± 0.84 , $P = 0.10$, Wilcoxon T). There was a significantly greater density of inhibitory terminals within the ventral and dorsal dendritic regions than observed in the cell body region in treated slices ($P < 0.002$ and $P < 0.02$, respectively). Scale bar = $20 \mu\text{m}$.

Local administration of ACM with heparin-acrylic beads

To examine the site of ACM action, we soaked heparin-acrylic beads in ACM and placed them just ventral to the NL cell layer, the site where GFAP-astrocytes first emerge at E15. The NL on one side received a bead coated in ACM, whereas the NL on the other side received a bead coated in control medium. In each case ($n = 4$) the density of VGAT puncta on the side that received the ACM coated bead was greater than the side with the control bead (Fig. 6). There was an increase of 3.4 puncta per $400 \mu\text{m}^2$ in the ventral dendritic region on the treated side (9.81 ± 2.01 per $400 \mu\text{m}^2$) compared to controls (6.41 ± 1.84 , $P < 0.05$, paired t -test; compare black arrows to white arrows in Fig. 6A',B', also Fig. 6C), and an increase of 2.6 per $400 \mu\text{m}^2$ in the dorsal dendritic neuropil (7.30 ± 2.32) compared to controls (4.68 ± 1.39 , $P < 0.05$, paired t -test; compare Fig. 6A,B, Fig. 6C). The density in the ventral and dorsal neuropil (9.81 and 7.30 , respectively; Fig. 6C) were not significantly different ($P = 0.08$, paired t -test), indicating diffusion of the ACM proteins to the dorsal extent of the organotypic slice.

The density within the cell body region was the lowest of all three regions, whether exposed to control medium (2.12 ± 0.55) or ACM supplemented medium (3.74 ± 0.93). However, unlike our observations when the entire slice was treated with ACM, the increase in VGAT density on cell bodies on the side with the ACM bead was significantly greater compared to the control side ($P < 0.05$, paired t -test; white arrowhead in Fig. 6B',C). Taken together, these data support a role for brainstem astrocyte-secreted molecules in increasing inhibitory inputs to NL.

DISCUSSION

In this study we characterized the development of inhibitory presynaptic terminals in NL and investigated the role of GFAP-positive astrocytes in the maturation of inhibitory projections in the auditory brainstem. We found that inhibitory inputs are first seen in NL at E9 and are initially more densely distributed within the ventral neuropil than dorsal neuropil. The density of VGAT puncta increases subsequently in development, with a significant increase in the density of VGAT puncta apposed to NL dendrites between E13–15 and E16–17. When we treated E13 organotypic brainstem slices with ACM from E16 brainstem astrocytes, we observed an increase in VGAT puncta that recapitulated the increase seen during normal development. These results suggest GFAP-positive astrocytes promote the maturation of inhibitory synapses in NL.

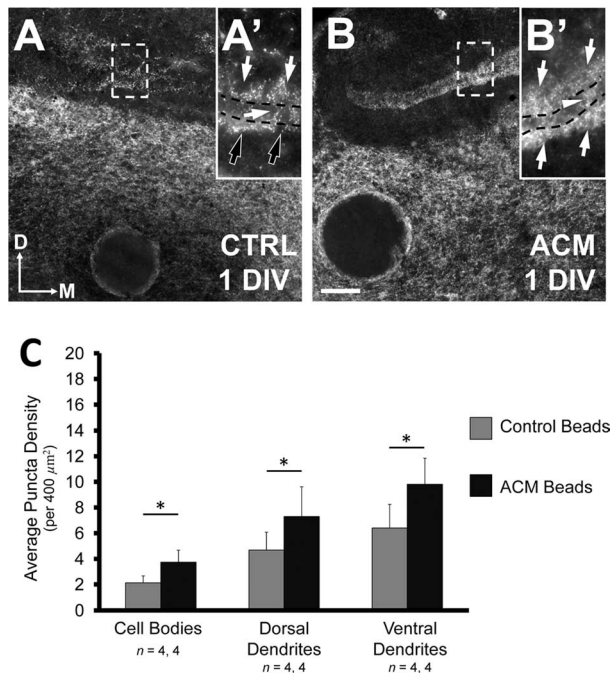


Figure 6. ACM-soaked beads increase the density of VGAT puncta in all NL regions. Figure shows an organotypic slice that received a control bead on one side (A) and a bead soaked in ACM on the other (B). A: Bead placement does not distort the NL cell layer. Consistent with results from slices incubated in control medium, the density of inhibitory terminals on the side of the slice with a bead soaked in control medium is less than that seen on the treated side. The ventral neuropil also exhibits a polarized distribution (A', black arrows), similar to that observed in control slices that received a full bath exchange of control medium. B: In contrast, sides with ACM-coated beads have a greater density of VGAT puncta than the control condition throughout NL. Dorsal and ventral dendritic regions contain similar densities of inhibitory terminals (B', white arrows). Unlike slices where ACM was included in the culture medium, the cell body region on the ACM bead sides has notably more inhibitory terminals than the control side (B', white arrowhead). C: The cell body region on the treated side had a significantly greater density of VGAT puncta (3.74 ± 0.93 puncta per $400 \mu\text{m}^2$) compared to the control side (2.12 ± 0.55 , $P < 0.05$). The ventral dendritic region exhibits a significantly greater density of inhibitory terminals (9.81 ± 2.01) compared to control slices (6.41 ± 1.84 , $P < 0.05$, paired t -test). The density of VGAT puncta on within the dorsal dendritic region on the ACM bead side (7.30 ± 2.32) was significantly greater than that seen on the control side (4.68 ± 1.39 , $P < 0.05$, paired t -test). This increase was sufficient to balance the density across dorsal and ventral neuropil regions ($P = 0.08$, paired t -test). Scale bar = $50 \mu\text{m}$ for A,B; $30 \mu\text{m}$ for A',B'.

Three phases of development of GABAergic synapses in NL

The earliest age that GABAergic terminals or cells have previously been identified in NL was E7 (von Bartheld et al., 1989), and these cells represented a population of GABAergic interneurons. Our data show that these cells provide only a minor contribution to VGAT terminals in

NL, as cutting SON axons eliminates VGAT labeling in the region (Fig. 1D).

Although the NL cell layer is not entirely laminated at E9, we detected putative terminals in the area around NL and, most notably, just ventral to the forming neuropil (Fig. 2A). This ventral side is proximal to the primary source of inhibitory terminals arising from the SON, located in the ventral brainstem (Lachica et al., 1994; Burger et al., 2005a). Consistent with previous studies (Code et al., 1989), we found that few VGAT puncta were seen in NL at E9, after which a first phase of substantial increase in inhibitory presynaptic puncta can be observed (Figs. 2A, 7A).

Phase I of inhibitory synapse development: emergence of presynaptic terminals

We identified GABAergic terminals on the cell bodies and dendritic regions in NL at E10–12 (phase I, Fig. 7A), consistent with previous reports (Code et al., 1989). At this age we found that VGAT puncta were significantly more numerous in the ventral neuropil than in the dorsal neuropil. This asymmetric distribution is reminiscent of the expression of TrkB, whose expression is confined to the ventral neuropil at E10 (Cochran et al., 1999; Cramer et al., 2000). Conversely, dorsal dendrites express the receptor tyrosine kinase receptor EphA4 at this age (Cramer et al., 2000), suggesting that distinct signals arise separately from the dorsal and ventral neuropil during the time that GABAergic terminals form contacts. Unlike the expression of EphA4, there does not appear to be a tonotopic gradient of VGAT labeling at any age. VGAT polarity (Figs. 2B, 7A) at E10 suggests either a delay in the arrival of SON axons to the dorsal region, or a relative delay in the time that presynaptic terminals differentiate in this region of NL.

Phase II of inhibitory synapse development: expansion of VGAT puncta

After this initial phase, we observed an increase in the density of VGAT puncta in NL, consistent with the appearance of GABAergic fibers noted in previous studies (Code et al., 1989; Code and Churchill, 1991). At E13–15 (phase II, Fig. 7B) there is an increase in VGAT density in both the dorsal and ventral neuropil; however, there is still a significantly greater VGAT density in the ventral NL dendrite region. Interestingly, there was no significant increase in density of VGAT puncta associated with a postsynaptic dendrite compared to phase I. This observation is consistent with the possibility that terminals express VGAT prior to becoming associated with postsynaptic cells (Fig. 7C).

Phase III of inhibitory synapse development: VGAT puncta apposed to NL dendrites

As previously reported, GABA terminals in NM (Code et al., 1989) and GABA_B receptors in NL (Burger et al.,

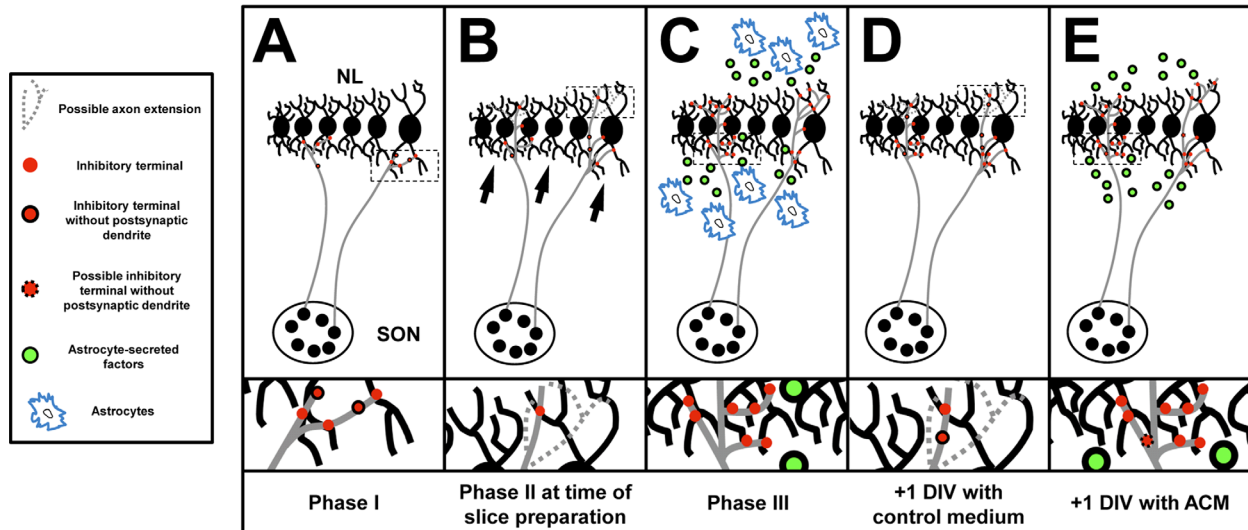


Figure 7. Summary of interactions that take place during development and in organotypic slice experiments. **A:** The first phase of inhibitory synaptogenesis is the period between E10–12. SON axons are in contact with neuron in NL and inhibitory terminals (red circles) just begin to populate the ventral neuropil and cell body layer. **B:** We place brainstem slices into culture during phase 2, at E13, prior to the emergence of GFAP-positive astrocytes. While there has been an increase in the number of terminals within the ventral and dorsal neuropil, there remains a pronounced asymmetry with a greater density of VGAT puncta in the ventral neuropil (black arrows). SON axon terminals may not extend into the dorsal neuropil (dashed axon extension), alternatively, or dorsally extending terminals may not yet express VGAT. Terminals may not yet be associated with a postsynaptic dendrite (red circles traced in black). **C:** After phase three (E16–17), inhibitory terminals are evenly distributed throughout both the ventral and dorsal dendritic regions. At this age GABAergic release sites are closely aligned with their dendritic targets and the synapses function to depolarize compartments of NL dendritic arbors. The density of terminals remains significantly less within the cell body region than in the cell-free neuropil. This distribution may be due, in part, to astrocytes (blue patches) that surround NL and secrete factors (green circles) that interact with NL cell bodies and their dendrites. **D:** After +1 DIV, in the absence of any astrocyte-secreted factors, there is a small increase in the number of terminals along the ventral neuropil and the imbalance between dorsal and ventral dendrites is still apparent. The number of VGAT puncta along NL dendrites has not changed. **E:** The last panel represents what we hypothesize results from astrocyte-secreted factors in the developing NL. SON axons have branched into the dorsal dendrite region and new terminals can be found along NL dendrites. Evidence presented here suggest that factors contained with ACM from GFAP-positive astrocyte isolated from E16 brainstems are capable of mimicking the developmental increase and distribution of inhibitory inputs to NL observed during the last phase of inhibitory synaptogenesis.

2005b) increase in number and take on a mature morphology in the brainstems from chickens E16 and older. At E16–17 (phase III in Fig. 7C) we observed a second significant increase in the number of VGAT-positive terminals and a shift in the distribution in the dorsal and ventral neuropil that results in similar density of terminals in dorsal and ventral dendritic regions (Fig. 7C).

At this late age we also observed a significant increase in the number of VGAT puncta per dendritic length. This change may indicate an increase in contacts formed by nascent inhibitory synapses and their targets in NL, and suggests that this phase of development is necessary for maturation of inhibitory synapses. Changes in the percent of NL dendrites covered with terminals coincides with reorganization of NL dendrites during this period of development (Smith and Rubel, 1979; Gray et al., 1982). Both changes may thus contribute to establishing the density and distribution of inhibitory synapses on NL dendrites.

This late phase of changes in VGAT distribution is likely associated with the final stages of maturation of

inhibitory inputs to NL. The distribution of VGAT puncta at E16–17 looks very similar to studies in posthatch and mature birds that use VGAT or the GABAergic recycling protein, GAD65, to label inhibitory synapses (Carr et al., 1989; Nishino et al., 2008; Tabor et al., 2010). GABA reversal potentials are stable (Lu and Trussell, 2001) and the tonic GABAergic shunting mechanism that relies on the GABA_AR- δ subunit is mature by E17 (Tang et al., 2011). In addition, NL neurons of late-age embryos have similar intrinsic properties as hatched animals, suggesting important elements of the auditory circuit are mature several days before hatching (Reyes et al., 1996; Funabiki et al., 1998; Yang et al., 1999). Thus, this last developmental phase may complete the maturation of inhibitory synapses in the avian auditory brainstem.

While most of the connections have formed at this phase, it remains possible that subsequent adjustments are made that reorganize the inhibitory sites. Substantial refinement has been reported in the mammalian lateral

superior olive (LSO; Sanes and Siverls, 1991; Kim and Kandler, 2003) and middle superior olive (MSO), where auditory experience results in the redistribution of inhibitory inputs to the cell body (Kapfer et al., 2002). The density of VGAT labeling becomes increasingly difficult to count reliably using our method at ages older than E17. Additional optical sectioning methods may be useful in future studies to look at the distribution of synapses in the mature NL.

VGAT density along the tonotopic axis

In addition to processing ITDs by having spatial segregated inputs, NM projections to NL are also topographically organized from rostromedial (high frequency) to caudolateral (low frequency) (Rubel and Parks, 1975; Young and Rubel, 1983; Lippe and Rubel, 1985), along a characteristic gradient of dendritic arbor size (Smith and Rubel, 1979). This arrangement makes NL uniquely equipped to process ITDs of different frequencies (Agmon-Snir et al., 1998; Kuba et al., 2005). More important, topographic organization can also be seen in the projections from SON to NL such that the neurons located in the ventral SON innervate the rostromedial region of NL, and the dorsal SON neurons the caudolateral NL (Tabor et al., 2010). Here we found that there was no tonotopic variation in the density of inhibitory inputs from SON at any of the ages examined through E17. These observations suggest that tonotopy does not influence the density of projections and that divergence from SON to regions of NL is uniform across the frequency axis.

Astrocyte-secreted proteins increase the density of GABAergic terminals in a manner that mimics normal development

The third phase of inhibitory maturation in NL occurs at a time when GFAP-positive astrocytes are maturing in NL (Korn and Cramer, 2008). While other glial cell types are present prior to this age, the close temporal correlation of this specific population led us to investigate whether the factors secreted from these astrocytes promote maturation of inhibition. We found significant differences between slices exposed to ACM compared to controls, evidence that indicates SON axons are receptive to factors isolated from our astrocyte population (Barker et al., 2008). It would follow, then, that receptors necessary for such interactions are likely present at E13.

After 24 hours of treatment, astrocyte-secreted factors are capable of increasing the density of GABAergic terminals throughout both the ventral and dorsal neuropil (Fig. 7E). When ACM is added to the culture medium, it is assumed that both ventral and dorsal neuropil receive equal concentrations of the factors of interest. In normal

development we observe that astrocytes first appear just ventral to NL and become in close proximity to the dorsal neuropil around E17 (Korn and Cramer, 2008). If we make the assumption that astrocytes interact with the terminal ends of SON axons rather than the postsynaptic neuron, we can interpret our results in two ways. In one interpretation, the initial polarity in VGAT labeling before the third phase of development results from secreted factors that do not diffuse sufficiently beyond the ventral neuropil to cause an effect. The density of inputs is later balanced on dorsal and ventral sides as astrocytes surround the cell layer, secreting factors that reach SON axons in both ventral and dorsal dendrites. Alternatively, astrocytes could be secreting one or more factors that disinhibit dorsally acting signaling molecules that prevent the invasion of inhibitory synapses prior to E16. However, these data alone do not exclude possibility that ACM and the astrocyte-secreted factors are acting on SON neuron cell bodies or on proximal regions of SON axons.

In order to determine where ACM exerts its effects, we used beads coated with ACM to administer a limited quantity of astrocyte-secreted proteins in the area directly adjacent to NL and at the same time distant from SON. Experiments using beads report a graded release of bound factors such that the concentration becomes progressively lower as the distance from the bead increases (Alexandre et al., 2006; Currel et al., 2007; Korn and Cramer, 2007). ACM beads in this study also increased the density of VGAT, suggesting that ACM factors act on SON terminals, rather than indirectly through SON cell bodies. These data are consistent with the possibility that ACM increases VGAT puncta at the terminals, and may also support a possible interaction with SON axons or their terminal branching (Fig. 7E).

Astrocyte-secreted factors: possible mechanisms

During the second phase of inhibitory synapse maturation, SON axons grow into NL, but terminals are restricted to the ventral portion of the nucleus (Fig. 7B). These observations suggest that either GABAergic proteins have not migrated to the dorsally oriented terminals (dashed axons, Fig. 7B,D) or that the axons themselves have not branched into the dorsal neuropil.

In the third phase of GABAergic development, the density of VGAT terminals becomes similar on both the ventral and dorsal neuropil. The data presented here support the hypothesis that astrocytes secrete factors that enhance the growth and branching of SON into the dorsal neuropil (Fig. 7E). This function would be consistent with recent studies showing that ACM not only enhances inhibitory synaptogenesis in dissociated hippocampal

neurons, but also increases GABAergic axon length and branching (Hughes et al., 2010). Alternatively, SON axons may already be present within the dorsal neuropil, and factors in ACM may promote an increase in the number of VGAT puncta in the dorsal neuropil. Either mechanism leads to a balance of inputs onto the dorsal and ventral sides of NL. Further studies are needed to examine if ACM factors that promote synaptogenesis also enhance the formation of contacts between VGAT terminals and their postsynaptic sites in NL.

Astrocyte-secreted factors modulate the developmental distribution of GABAergic terminals

There are several reports on the role of glia during the maturation of excitatory synaptogenesis (Pfrieger and Barres, 1997; Nagler et al., 2001; Mauch et al., 2001; Ullian et al., 2004; Christopherson et al., 2005; Colon-Ramos et al., 2007; Eroglu, 2009; Eroglu et al., 2009). Relatively little is known about the role of glia in the maturation of inhibitory synapses, and these studies are generally limited to interactions in dissociated hippocampal cultures (Liu et al., 1997; Liu et al., 1996; Elmariah et al., 2004). Thrombospondins (TSPs) are necessary for neuron-glia interactions when forming glutamatergic synapses (Hughes et al., 2010), but have only a limited homeostatic role in affecting inhibitory synaptogenesis (Duveau et al., 2011). Although there is some indication that astrocytes may be involved in the modulation of TrkB signaling, which is necessary for functioning inhibitory synapses (Elmariah et al., 2005a,b), it is not clear when and to what extent these interactions are required. In this study we provide evidence that ACM influences formation of inhibitory synapses in the organotypic auditory brainstem preparation. These results are consistent with the possibility that astrocytes have a broad role in inhibitory synaptogenesis throughout the central nervous system.

Distribution of inhibitory inputs in NL

The distribution of inhibitory inputs to somata and dendritic regions of NL represents a divergence from the arrangement seen in a mammalian nucleus analogous to NL, the medial superior olive (MSO) (Lesica et al., 2010; Ashida and Carr, 2011). In gerbils, chinchillas, and cats, MSO neurons receive glycinergic inputs restricted to the somata (Clark, 1969; Perkins, 1973; Adams and Mugnaini, 1990; Kapfer et al., 2002). In the avian auditory system, where GABA is the primary inhibitory source in NL (Carr et al., 1989; Overholt et al., 1992; Yang et al., 1999; Burger et al., 2005a), inhibition is distributed throughout NL neurons. Our data indicate that GABAergic terminals first appear on NL dendrites, with a significantly lower

density on the cell body. Although the density does increase within the cell body region during the third phase of maturation, the dendrites maintain a higher density of VGAT terminals. It should be noted that although we used VGAT as a marker for terminals that release GABA, thought to be the predominant inhibitory neurotransmitter in the avian auditory brainstem, there is some evidence that both GABA and glycine are released from VGAT terminals in the auditory brainstem (Kuo et al., 2009; Coleman et al., 2011). It is thus possible that our puncta contain a mixed population of inhibitory terminals.

Modeling studies illustrate that NL neurons become more efficient at coincidence detection in part by processing low frequencies onto neurons with longer, bipolar dendrites (Agmon-Snir et al., 1998; Grau-Serrat et al., 2003; Dasika et al., 2007). Complex dendritic arbors, by branching and/or length, improve precision in coincidence detection (Takigawa-Imamura and Motoike, 2011). GABAergic inputs depolarize NL neurons, stimulating low-threshold K^+ channels, which then increase the resistance and decreases the excitability within the local dendritic compartment (Hyson et al., 1995; Yang et al., 1999; Dasika et al., 2005; Hyson, 2005). The distribution of Ca^{2+} channels throughout the dendrites supports the hypothesis that dendritic segments of NL neurons are compartmentalized units that must be dynamically regulated to process temporally sensitive and phase-locked information (Blackmer et al., 2009). In contrast to MSO, inhibition enhances precision by being distributed along cell bodies and dendrites in NL.

These studies suggest that the spatial distribution of inhibitory inputs to NL provide significant control over the function of these neurons in computing interaural time differences. Here we characterized the emergence of these inputs over the course of development. The role of astrocytes suggests that glial cells provide important cues during the formation of precise auditory circuitry.

ACKNOWLEDGMENT

The authors would like to thank Dr. Candace Hsieh and Minhan Dinh for their technical expertise.

LITERATURE CITED

- Adams JC, Mugnaini E. 1990. Immunocytochemical evidence for inhibitory and disinhibitory circuits in the superior olive. *Hear Res* 49:281–298.
- Agmon-Snir H, Carr CE, Rinzel J. 1998. The role of dendrites in auditory coincidence detection. *Nature* 393:268–272.
- Alexandre P, Bachy I, Marcou M, Wassef M. 2006. Positive and negative regulations by FGF8 contribute to midbrain roof plate developmental plasticity. *Development* 133: 2905–2913.
- Ashida G, Carr CE. 2011. Sound localization: Jeffress and beyond. *Curr Opin Neurobiol* [Epub ahead of print].

- Barker AJ, Koch SM, Reed J, Barres BA, Ullian EM. 2008. Developmental control of synaptic receptivity. *J Neurosci* 28: 8150–8160.
- Blackmer T, Kuo SP, Bender KJ, Apostolides PF, Trussell LO. 2009. Dendritic calcium channels and their activation by synaptic signals in auditory coincidence detector neurons. *J Neurophysiol* 102:1218–1226.
- Book KJ, Morest DK. 1990. Migration of neuroblasts by perikaryal translocation: role of cellular elongation and axonal outgrowth in the acoustic nuclei of the chick embryo medulla. *J Comp Neurol* 297:55–76.
- Bruckner S, Hyson RL. 1998. Effect of GABA on the processing of interaural time differences in nucleus laminaris neurons in the chick. *Eur J Neurosci* 10:3438–3450.
- Burger RM, Cramer KS, Pfeiffer JD, Rubel EW. 2005a. Avian superior olivary nucleus provides divergent inhibitory input to parallel auditory pathways. *J Comp Neurol* 481:6–18.
- Burger RM, Pfeiffer JD, Westrum LE, Bernard A, Rubel EW. 2005b. Expression of GABA(B) receptor in the avian auditory brainstem: ontogeny, afferent deprivation, and ultrastructure. *J Comp Neurol* 489:11–22.
- Carr CE, Konishi M. 1990. A circuit for detection of interaural time differences in the brain stem of the barn owl. *J Neurosci* 10:3227–3246.
- Carr CE, Fujita I, Konishi M. 1989. Distribution of GABAergic neurons and terminals in the auditory system of the barn owl. *J Comp Neurol* 286:190–207.
- Chaudhry FA, Reimer RJ, Bellocchio EE, Danbolt NC, Osen KK, Edwards RH, Storm-Mathisen J. 1998. The vesicular GABA transporter, VGAT, localizes to synaptic vesicles in sets of glycinergic as well as GABAergic neurons. *J Neurosci* 18: 9733–9750.
- Cheng SM, Carr CE. 2007. Functional delay of myelination of auditory delay lines in the nucleus laminaris of the barn owl. *Dev Neurobiol* 67:1957–1974.
- Christopherson KS, Ullian EM, Stokes CC, Mallowney CE, Hell JW, Agah A, Lawler J, Mosher DF, Bornstein P, Barres BA. 2005. Thrombospondins are astrocyte-secreted proteins that promote CNS synaptogenesis. *Cell* 120:421–433.
- Clark GM. 1969. The ultrastructure of nerve endings in the medial superior olive of the cat. *Brain Res* 14:293–305.
- Cochran SL, Stone JS, Bermingham-McDonogh O, Akers SR, Lefcort F, Rubel EW. 1999. Ontogenetic expression of trk neurotrophin receptors in the chick auditory system. *J Comp Neurol* 413:271–288.
- Code RA, Churchill L. 1991. GABAA receptors in auditory brainstem nuclei of the chick during development and after cochlea removal. *Hear Res* 54:281–295.
- Code RA, Rubel EW. 1989. Glycine-immunoreactivity in the auditory brain stem of the chick. *Hear Res* 40:167–172.
- Code RA, Burd GD, Rubel EW. 1989. Development of GABA immunoreactivity in brainstem auditory nuclei of the chick: ontogeny of gradients in terminal staining. *J Comp Neurol* 284:504–518.
- Coleman WL, Fischl MJ, Weimann SR, Burger RM. 2011. GABAergic and glycinergic inhibition modulate monaural auditory response properties in the avian superior olivary nucleus. *J Neurophysiol* 105:2405–2420.
- Colon-Ramos DA, Margeta MA, Shen K. 2007. Glia promote local synaptogenesis through UNC-6 (netrin) signaling in *C. elegans*. *Science* 318:103–106.
- Cramer KS, Rosenberger MH, Frost DM, Cochran SL, Pasquale EB, Rubel EW. 2000. Developmental regulation of EphA4 expression in the chick auditory brainstem. *J Comp Neurol* 426:270–278.
- Currle DS, Kolski-Andreaco A, Monuki ES. 2007. Growth factor-coated bead placement on dorsal forebrain explants. *J Vis Exp* 134.
- Dasika VK, White JA, Carney LH, Colburn HS. 2005. Effects of inhibitory feedback in a network model of avian brain stem. *J Neurophysiol* 94:400–414.
- Dasika VK, White JA, Colburn HS. 2007. Simple models show the general advantages of dendrites in coincidence detection. *J Neurophysiol* 97:3449–3459.
- Deitch JS, Rubel EW. 1989. Changes in neuronal cell bodies in N. laminaris during deafferentation-induced dendritic atrophy. *J Comp Neurol* 281:259–268.
- Duveau V, Laustela S, Barth L, Gianolini F, Vogt KE, Keist R, Chandra D, Homanics GE, Rudolph U, Fritschy JM. 2011. Spatiotemporal specificity of GABA(A) receptor-mediated regulation of adult hippocampal neurogenesis. *Eur J Neurosci* 34:362–373.
- Elmariah SB, Crumling MA, Parsons TD, Balice-Gordon RJ. 2004. Postsynaptic TrkB-mediated signaling modulates excitatory and inhibitory neurotransmitter receptor clustering at hippocampal synapses. *J Neurosci* 24:2380–2393.
- Elmariah SB, Hughes EG, Oh EJ, Balice-Gordon RJ. 2005a. Neurotrophin signaling among neurons and glia during formation of tripartite synapses. *Neuron Glia Biol* 1:1–11.
- Elmariah SB, Oh EJ, Hughes EG, Balice-Gordon RJ. 2005b. Astrocytes regulate inhibitory synapse formation via Trk-mediated modulation of postsynaptic GABAA receptors. *J Neurosci* 25:3638–3650.
- Eroglu C. 2009. The role of astrocyte-secreted matricellular proteins in central nervous system development and function. *J Cell Commun Signal* 3:167–176.
- Eroglu C, Allen NJ, Susman MW, O'Rourke NA, Park CY, Ozkan E, Chakraborty C, Mulinyawe SB, Annis DS, Huberman AD, Green EM, Lawler J, Dolmetsch R, Garcia KC, Smith SJ, Luo ZD, Rosenthal A, Mosher DF, Barres BA. 2009. Gabapentin receptor alpha2delta-1 is a neuronal thrombospondin receptor responsible for excitatory CNS synaptogenesis. *Cell* 139:380–392.
- Feng JJ, Morest DK. 2006. Development of synapses and expression of a voltage-gated potassium channel in chick embryonic auditory nuclei. *Hear Res* 216–217:116–126.
- Fujita I, Konishi M. 1991. The role of GABAergic inhibition in processing of interaural time difference in the owl's auditory system. *J Neurosci* 11:722–739.
- Fukui I, Burger RM, Ohmori H, Rubel EW. 2010. GABAergic inhibition sharpens the frequency tuning and enhances phase locking in chicken nucleus magnocellularis neurons. *J Neurosci* 30:12075–12083.
- Funabiki K, Koyano K, Ohmori H. 1998. The role of GABAergic inputs for coincidence detection in the neurons of nucleus laminaris of the chick. *J Physiol* 508(Pt 3):851–869.
- Gorlich A, Illy M, Friauf E, Wagner H, Luksch H, Lohrke A. 2010. Development of the delay lines in the nucleus laminaris of the chicken embryo revealed by optical imaging. *Neuroscience* 168:564–572.
- Grau-Serrat V, Carr CE, Simon JZ. 2003. Modeling coincidence detection in nucleus laminaris. *Biol Cybern* 89:388–396.
- Gray L, Smith Z, Rubel EW. 1982. Developmental and experimental changes in dendritic symmetry in n. laminaris of the chick. *Brain Res* 244:360–364.
- Harris J, Ayyub C, Shaw G. 1991. A molecular dissection of the carboxyterminal tails of the major neurofilament subunits NF-M and NF-H. *J Neurosci Res* 30:47–62.
- Hendricks SJ, Rubel EW, Nishi R. 2006. Formation of the avian nucleus magnocellularis from the auditory anlage. *J Comp Neurol* 498:433–442.
- Hughes EG, Elmariah SB, Balice-Gordon RJ. 2010. Astrocyte secreted proteins selectively increase hippocampal GABAergic axon length, branching, and synaptogenesis. *Mol Cell Neurosci* 43:136–145.
- Hyson RL. 2005. The analysis of interaural time differences in the chick brain stem. *Physiol Behav* 86:297–305.

- Hyson RL, Reyes AD, Rubel EW. 1995. A depolarizing inhibitory response to GABA in brainstem auditory neurons of the chick. *Brain Res* 677:117–126.
- Jhaveri S, Morest DK. 1982. Neuronal architecture in nucleus magnocellularis of the chicken auditory system with observations on nucleus laminaris: a light and electron microscope study. *Neuroscience* 7:809–836.
- Joseph AW, Hyson RL. 1993. Coincidence detection by binaural neurons in the chick brain stem. *J Neurophysiol* 69:1197–1211.
- Kapfer C, Seidl AH, Schweizer H, Grothe B. 2002. Experience-dependent refinement of inhibitory inputs to auditory coincidence-detector neurons. *Nat Neurosci* 5:247–253.
- Kim G, Kandler K. 2003. Elimination and strengthening of glycinergic/GABAergic connections during tonotopic map formation. *Nat Neurosci* 6:282–290.
- Korn MJ, Cramer KS. 2007. Placing growth factor-coated beads on early stage chicken embryos. *J Vis Exp* 307.
- Korn MJ, Cramer KS. 2008. Distribution of glial-associated proteins in the developing chick auditory brainstem. *Dev Neurobiol* 68:1093–1106.
- Kuba H, Yamada R, Fukui I, Ohmori H. 2005. Tonotopic specialization of auditory coincidence detection in nucleus laminaris of the chick. *J Neurosci* 25:1924–1934.
- Kuenzel T, Monig B, Wagner H, Mey J, Luksch H. 2007. Neuronal differentiation of the early embryonic auditory hindbrain of the chicken in primary culture. *Eur J Neurosci* 25:974–984.
- Kuo SP, Bradley LA, Trussell LO. 2009. Heterogeneous kinetics and pharmacology of synaptic inhibition in the chick auditory brainstem. *J Neurosci* 29:9625–9634.
- Lachica EA, Rubsamen R, Rubel EW. 1994. GABAergic terminals in nucleus magnocellularis and laminaris originate from the superior olivary nucleus. *J Comp Neurol* 348:403–418.
- Lesica NA, Lingner A, Grothe B. 2010. Population coding of interaural time differences in gerbils and barn owls. *J Neurosci* 30:11696–11702.
- Lieberburg I, Spinner N, Snyder S, Anderson J, Goldgaber D, Smulowitz M, Carroll Z, Emanuel B, Breitner J, Rubin L. 1989. Cloning of a cDNA encoding the rat high molecular weight neurofilament peptide (NF-H): developmental and tissue expression in the rat, and mapping of its human homologue to chromosomes 1 and 22. *Proc Natl Acad Sci U S A* 86:2463–2467.
- Lippe W, Rubel EW. 1985. Ontogeny of tonotopic organization of brain stem auditory nuclei in the chicken: implications for development of the place principle. *J Comp Neurol* 237:273–289.
- Lippe WR, Steward O, Rubel EW. 1980. The effect of unilateral basilar papilla removal upon nuclei laminaris and magnocellularis of the chick examined with [3H]2-deoxy-D-glucose autoradiography. *Brain Res* 196:43–58.
- Liu QY, Schaffner AE, Li YX, Dunlap V, Barker JL. 1996. Up-regulation of GABA current by astrocytes in cultured embryonic rat hippocampal neurons. *J Neurosci* 16:2912–2923.
- Liu QY, Schaffner AE, Chang YH, Vasil K, Barker JL. 1997. Astrocytes regulate amino acid receptor current densities in embryonic rat hippocampal neurons. *J Neurobiol* 33:848–864.
- Lu T, Trussell LO. 2001. Mixed excitatory and inhibitory GABA-mediated transmission in chick cochlear nucleus. *J Physiol* 535(Pt 1):125–131.
- Lurie DI, Rubel EW. 1994. Astrocyte proliferation in the chick auditory brainstem following cochlea removal. *J Comp Neurol* 346:276–288.
- Lurie DI, Solca F, Fischer EH, Rubel EW. 2000. Tyrosine phosphatase SHP-1 immunoreactivity increases in a subset of astrocytes following deafferentation of the chicken auditory brainstem. *J Comp Neurol* 421:199–214.
- Mauch DH, Nagler K, Schumacher S, Goritz C, Muller EC, Otto A, Pfrieger FW. 2001. CNS synaptogenesis promoted by glia-derived cholesterol. *Science* 294:1354–1357.
- Monsivais P, Yang L, Rubel EW. 2000. GABAergic inhibition in nucleus magnocellularis: implications for phase locking in the avian auditory brainstem. *J Neurosci* 20:2954–2963.
- Müller CM. 1987. gamma-Aminobutyric acid immunoreactivity in brainstem auditory nuclei of the chicken. *Neurosci Lett* 77:272–276.
- Nagler K, Mauch DH, Pfrieger FW. 2001. Glia-derived signals induce synapse formation in neurons of the rat central nervous system. *J Physiol* 533(Pt 3):665–679.
- Nguyen QT, Callamaras N, Hsieh C, Parker I. 2001. Construction of a two-photon microscope for video-rate Ca(2+) imaging. *Cell Calcium* 30:383–393.
- Nishino E, Yamada R, Kuba H, Hioki H, Furuta T, Kaneko T, Ohmori H. 2008. Sound-intensity-dependent compensation for the small interaural time difference cue for sound source localization. *J Neurosci* 28:7153–7164.
- Overholt EM, Rubel EW, Hyson RL. 1992. A circuit for coding interaural time differences in the chick brainstem. *J Neurosci* 12:1698–1708.
- Perkins RE. 1973. An electron microscopic study of synaptic organization in the medial superior olive of normal and experimental chinchillas. *J Comp Neurol* 148:387–415.
- Person AL, Cerretti DP, Pasquale EB, Rubel EW, Cramer KS. 2004. Tonotopic gradients of Eph family proteins in the chick nucleus laminaris during synaptogenesis. *J Neurobiol* 60:28–39.
- Pfrieger FW, Barres BA. 1997. Synaptic efficacy enhanced by glial cells in vitro. *Science* 277:1684–1687.
- Reyes AD, Rubel EW, Spain WJ. 1996. In vitro analysis of optimal stimuli for phase-locking and time-delayed modulation of firing in avian nucleus laminaris neurons. *J Neurosci* 16:993–1007.
- Rubel EW, Parks TN. 1975. Organization and development of brain stem auditory nuclei of the chicken: tonotopic organization of n. magnocellularis and n. laminaris. *J Comp Neurol* 164:411–433.
- Rubel EW, Smith DJ, Miller LC. 1976. Organization and development of brain stem auditory nuclei of the chicken: ontogeny of n. magnocellularis and n. laminaris. *J Comp Neurol* 166:469–489.
- Sanchez JT, Wang Y, Rubel EW, Barria A. 2010. Development of glutamatergic synaptic transmission in binaural auditory neurons. *J Neurophysiol* 104:1774–1789.
- Sanchez JT, Seidl AH, Rubel EW, Barria A. 2011. Preparation and culture of chicken auditory brainstem slices. *J Vis Exp pii:2527*.
- Sanes DH, Siverls V. 1991. Development and specificity of inhibitory terminal arborizations in the central nervous system. *J Neurobiol* 22:837–854.
- Seidl AH, Rubel EW. 2009. A simple method for multiday imaging of slice cultures. *Microsc Res Tech* 73:37–44.
- Seidl AH, Rubel EW, Harris DM. 2010. Mechanisms for adjusting interaural time differences to achieve binaural coincidence detection. *J Neurosci* 30:70–80.
- Smith DJ, Rubel EW. 1979. Organization and development of brain stem auditory nuclei of the chicken: dendritic gradients in nucleus laminaris. *J Comp Neurol* 186:213–239.
- Sorensen SA, Rubel EW. 2006. The level and integrity of synaptic input regulates dendrite structure. *J Neurosci* 26:1539–1550.
- Stutzmann GE, Parker I. 2005. Dynamic multiphoton imaging: a live view from cells to systems. *Physiology (Bethesda)* 20:15–21.
- Stutzmann GE, LaFerla FM, Parker I. 2003. Ca²⁺ signaling in mouse cortical neurons studied by two-photon imaging and photoreleased inositol triphosphate. *J Neurosci* 23:758–765.

- Tabor KM, Wong RO, Rubel EW. 2010. Topography and morphology of the inhibitory projection from superior olivary nucleus to nucleus laminaris in chickens (*Gallus gallus*). *J Comp Neurol* 519:358–375.
- Takigawa-Imamura H, Motoike IN. 2011. Dendritic gates for signal integration with excitability-dependent responsiveness. *Neural Netw* [Epub ahead of print].
- Tang ZQ, Dinh EH, Shi W, Lu Y. 2011. Ambient GABA-activated tonic inhibition sharpens auditory coincidence detection via a depolarizing shunting mechanism. *J Neurosci* 31: 6121–6131.
- Taylor AR, Robinson MB, Milligan CE. 2007. In vitro methods to prepare astrocyte and motoneuron cultures for the investigation of potential in vivo interactions. *Nat Protoc* 2: 1499–1507.
- Ullian EM, Christopherson KS, Barres BA. 2004. Role for glia in synaptogenesis. *Glia* 47:209–216.
- von Bartheld CS, Code RA, Rubel EW. 1989. GABAergic neurons in brainstem auditory nuclei of the chick: distribution, morphology, and connectivity. *J Comp Neurol* 287: 470–483.
- Westerberg BD, Schwarz DW. 1995. Connections of the superior olive in the chicken. *J Otolaryngol* 24:20–30.
- Yang L, Monsivais P, Rubel EW. 1999. The superior olivary nucleus and its influence on nucleus laminaris: a source of inhibitory feedback for coincidence detection in the avian auditory brainstem. *J Neurosci* 19:2313–2325.
- Young SR, Rubel EW. 1983. Frequency-specific projections of individual neurons in chick brainstem auditory nuclei. *J Neurosci* 3:1373–1378.